

Optimal Design of Microfluidic Devices for Rapid DNA Separations

Max A. Fahrenkopf* B. Erik Ydstie*,** Tamal Mukherjee**
James W. Schneider*

* *Department of Chemical Engineering,*

** *Department of Electrical and Computer Engineering,
Carnegie Mellon University, Pittsburgh, PA 15213 USA*

*email: mfahrenk@andrew.cmu.edu, ydstie@cmu.edu,
tamal@ece.cmu.edu, schneider@cmu.edu*

Abstract: DNA separation is required to be rapid to be a useful component in DNA analysis devices. Different microfluidic device structures can be exploited to separate DNA with high throughput. We presents a framework for determining the optimal microfluidic device structure for rapid DNA separation through solving a nonlinear programming problem. Optimally designed spiral and serpentine microfluidic device configurations are shown to give comparable results for separating up to 425 bases of DNA using the micelle end-labeled free solution electrophoresis technique. The minimum run time for the serpentine microfluidic device configuration separating up to 425 bases of DNA is 5.1 minutes.

Keywords: Optimization, Nonlinear Programming, Biotechnology, DNA separation, Microfluidics

1. INTRODUCTION

DNA separation is an essential step in many DNA analysis techniques including DNA sequencing (Sanger et al., 1977), cancer identification (Albrecht et al., 2013) and forensic analysis (Butler, 2001). DNA separation by electrophoresis, when coupled with micelle chromatography, forms a fast and reliable method called micelle end-labeled free-solution electrophoresis (ELFSE) (Grosser et al., 2007; Savard et al., 2008). Micelle ELFSE is well suited for microfluidic devices, which are commonly used for electrophoretic separations of small samples sizes on order of $1 \mu\text{L}$ and holds several advantages for rapid separations over conventional bench-top capillary electrophoresis methods.

Design variables such as micelle size, applied electric field strength, and microfluidic device layout are not easily identified by intuition and laboratory experience alone. Several groups have worked in the area of modeling (Culbertson et al., 1998; Griffiths and Nilson, 2000; Molho et al., 2001; Wang et al., 2004) and optimization of electrokinetic separations using microfluidic devices (Pfeiffer et al., 2004). In this paper we develop a modeling and optimization framework for rapid DNA separations on a microfluidic device using micelle ELFSE. Our optimization approach allows for assessment of different microfluidic device configurations. The two configurations considered in this work are spirals and serpentes. The trade-offs between spirals and serpentes are discussed for DNA separation using micelle ELFSE and we conclude the serpentes is the optimal configuration in the sense of minimum run time.

2. MODELING AND OPTIMIZATION FRAMEWORK FOR DNA SEPARATION IN MICROFLUIDICS

In this section we outline the physics, modeling and optimization of the DNA separation problem on a microfluidic device. Electrophoretic separation of different lengths of DNA in a microfluidic device requires each DNA length to migrate at different velocities as determined by Eq. (1)

$$u = \mu E_{app} \quad (1)$$

where u is the velocity, E_{app} is the applied electric field, and μ is the electrophoretic mobility. The applied electric field is the ratio of the applied voltage to the channel length

$$E_{app} = V_{app}/L \quad (2)$$

The electrophoretic mobility μ is indicative of the number of charges on the analyte relative to the friction applied by the solvent to the analyte. For DNA, the number of charges and the friction applied by the solvent both increase linearly with increasing DNA length resulting in an electrophoretic mobility that scale independently of length (Viovy, 2000; Dorfman, 2010). Several methods exist to break the length independent scaling of DNA electrophoretic mobility. Micelle end-labeled free-solution electrophoresis is one such method that uses an uncharged surfactant micelle attached to the end of each DNA molecule to supply additional friction which scales as an affine function (linearly plus a constant) with increasing DNA length. The electrophoretic mobility, μ_m , of the micelle-DNA complex is

$$\mu_m = \mu_0 \frac{m}{m + \alpha} \quad (3)$$

where μ_0 is the free-solution mobility of DNA, m is the length of DNA in bases, and α is the size of the micelle in units of uncharged DNA bases that have the equivalent

drag of the micelle. The sensitivity of the mobility to DNA length $\partial\mu/\partial m$ is maximized when $\alpha = m$, while the mobility itself tends to zero as the micelle size, α , becomes large. As separation of long DNA lengths requires a large micelle of commensurate drag, the short DNA lengths will move very slowly.

As the DNA molecules migrate down the separation channel, they separate into different concentration profiles that are Gaussian in shape, when averaged across the cross-section of the separation channel, as shown in Figure 1. The concentration profiles are resolved from each other

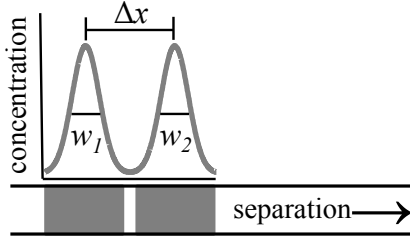


Fig. 1. Microfluidic separation processes produce Gaussian concentration profiles.

when the average full-width at half-maximum, w_m , is less than 1.5 times the spacing between maximums, Δx_m ,

$$R_m = \frac{w_m + w_{m+1}}{2\Delta x_m} \leq 1.5 \quad (4)$$

where R_m is the resolution factor. Well-resolved Gaussian profiles are identified using post-processing software that fit Gaussians to the detected concentration profiles. The spacing between Gaussians is given by

$$\Delta x_m = (\mu_{m+1} - \mu_m) E_{app} t \quad (5)$$

where t is the time at which the Gaussians are detected. The full-width at half-maximum is determined completely by the Gaussian's variance

$$w_m = 2\sqrt{2\ln(2)\sigma_m^2} \quad (6)$$

where σ_m^2 is the variance of each DNA length. The variance is a result of the disturbances that cause each DNA of length m to be at a slightly different position during detection. Separation devices are therefore built to mitigate against these different disturbance. If a separation device were ideal, the only source of variance would be due to diffusion, which is unavoidable according to the laws of Thermodynamics,

$$\sigma_{diff}^2 = 2Dt \quad (7)$$

where D is the DNA diffusivity, which scales with DNA length as $D = D_1/\sqrt{m + \alpha}$, and t is the mean detection time for DNA of length m . As variance due to diffusion grows with time, we generally want to design devices which require the least amount of time to achieve resolution. In micelle ELFSE DNA separations, the long DNA migrates the fastest so we would like to image the separation as soon as the long DNA becomes resolved. This can be achieved using snap-shot detection which images an entire separation channel at specific instant in time. Classically separations are detected using a finish-line detector which would require DNA of every length to pass a fixed location to be detected. Finish-line detection mode introduces a dead-time for micelle ELFSE DNA separations where the short DNA, which is the easiest to resolve, migrates to the detector at the slowest rate. Snap-shot detection

eliminates this dead-time by imaging the entire separation channel the instant the long DNA, and every shorter DNA length, is resolved. Snap-shot detection is difficult to implement, however, as it requires a small chip area due to optical constraints Dorfman et al. (2012). Sufficiently long separation channels, needed to achieve resolution, require that the separation channels curve to fit on a small area for the snap-shot detector.

Microfluidic devices are useful for DNA separations because they enable rapid detection of short DNA lengths by using a small topology to achieve "snap-shot" detections. Microfluidic devices are generally made on the top of a silicon or glass substrate and feature small channels (widths on the order of μm) etched in by acid or other lithography techniques Dorfman et al. (2012). Figure 2 shows the serpentine and spiral configurations which are commonly used to fit long separation channels on a small chip area. The convection-diffusion equation can be used to

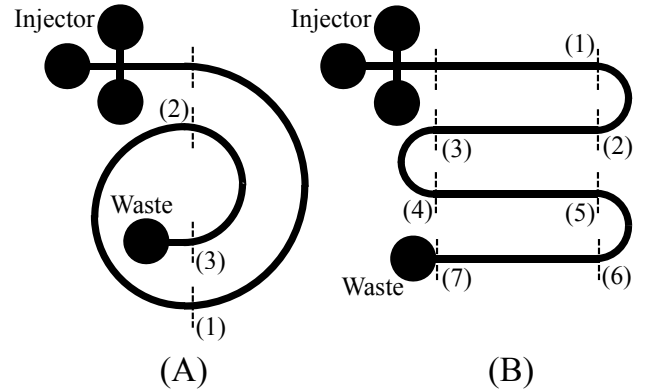


Fig. 2. (A) Microfluidic spiral, (B) microfluidic serpentine. The microfluidic devices each feature injection and waste reservoirs. Spirals are typically designed using connected semi-circles of decreasing radii. Serpentine feature both straight and turn sections. Each section is number and separated by a dashed line.

model the effect of the microfluidic device topology on the concentration profiles as the DNA lengths migrate through the microfluidic device

$$\frac{\partial c_m}{\partial t} + \mathbf{u} \cdot \nabla c_m = D \nabla^2 c_m \quad (8)$$

where c_m is the concentration profile of DNA of length m , D is the diffusivity, and \mathbf{u} is the electrophoretic velocity vector. The convection-diffusion equation (8) can be solved analytically, using a few simplifying assumptions, to reveal the model for the variance generation σ_m^2 as the concentration profile propagates down the microfluidic channel Griffiths and Nilson (2000); Molho et al. (2001); Wang et al. (2004).

The primary simplification to the convection diffusion equation (8) deals with the velocity of the DNA in a curved microfluidic channel. In a straight channel, the velocity is constant. In a microfluidic turns, the DNA velocity varies across the interior of the channel. This is because the outside channel has a longer contour length than the inside channel which also results in an electric field gradient. Defining the x coordinate to be along the axial direction of the microfluidic channel and the y coordinate to be

pointing to the interior of the microfluidic channel (see figure 3), the velocity is given by $\mathbf{u} = u(y)\mathbf{e}_x$ where \mathbf{e}_x is the unit vector pointing in the axial direction (Griffiths and Nilson, 2000; Molho et al., 2001; Wang et al., 2004).

The convection-diffusion equation (8) is two-dimensional in (x, y) and is solved analytically to determine σ_m^2 as a function of the microfluidic structure (Molho et al., 2001; Wang et al., 2004),

$$\sigma_m^2 = \sigma_0^2 + 2Dt + \sum_{i \in I} \sigma_{skew,i}^2 + \sum_{j \in J} \sigma_{turn,j}^2 + \sigma_{other}^2 \quad (9)$$

where σ_0^2 is the initial variance of the injected Gaussian profile, $2Dt$ is the variance caused by diffusion over the migration time t , DNA diffusivity scales as $D = D_1/\sqrt{m + \alpha}$ where D_1 is constant (Ren et al., 1999), $\sigma_{skew,i}^2$ is the variance caused by a skewed concentration profile as it enters section i , I is the set of all sections in the microfluidic device, $\sigma_{turn,j}^2$ is the variance caused by the concentration profile migrating through each turn, J is the set of all turn sections in the microfluidic device, and σ_{other}^2 is any other source of variance not modeled by the convective-diffusion equation. Here a section is defined as either a straight channel or a semi-circular turn. A spiral consists only of semi-circular turn sections while a serpentine

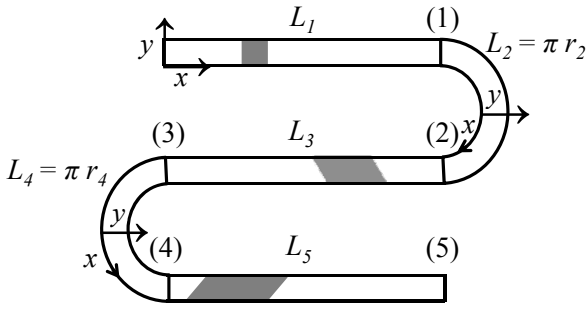


Fig. 3. Concentration profiles are broadened by turns. The variance of the concentration profile is increased during each turn and quantified by $\sigma_{turn,j}^2$. The initial concentration profile is unskewed. After the first turn the concentration profile becomes skewed and diffusion is enhanced by the concentration gradient which results in variance generation $\sigma_{skew,3}^2$. The second turn is complementary which subtracts some variance $\sigma_{skew,4}^2$. The index of each section i is specified at the section exit.

Figure 3 shows the variance generated by turns in a microfluidic device. After a turn, the concentration band becomes skewed. The skewed concentration band causes the variance to increase as the concentration gradient cause diffusion to be exacerbated. The variance increase due to concentration profile skew is

$$\sigma_{skew,i}^2 = \sum_{n=1,3,5,\dots}^{\infty} S_n^{(i)} \Gamma_n^{(i)} \quad (10)$$

where $\Gamma_n^{(i)} = \pm \frac{8\mu_m E_{app} w_c^2}{r_i D (n\pi)^4} \left(1 - e^{-(n\pi)^2 D t_i / w_c^2}\right)$, μ_m is the mobility given by Eq. (3), E_{app} is the applied electric field, w_c is the channel width, r_i is the radius of the center-line of the turn, D is the diffusivity, t_i is the time it takes to get through the turn or straight section i , i.e. $t_i = L_i / (\mu E_{app})$ where L_i is length of the turn or straight channel. The term

$S_n^{(i)}$ indicates the concentration band skewness as it enters section i .

$$S_n^{(i)} = \begin{cases} S_n^{(i-1)} e^{-(n\pi)^2 D t_{i-1} / w_c^2}, & (i-1) \in K \\ S_n^{(i-1)} e^{-(n\pi)^2 D t_{i-1} / w_c^2} + \Gamma_n^{(i-1)}, & (i-1) \in J \end{cases} \quad (11)$$

where K is the set of straight sections, J is the set of turn sections, and the initial concentration profile is assumed to be unskewed, $S_n^{(1)} = 0$. The sign on the terms $\sigma_{skew,i}^2$ and $\Gamma_n^{(i)}$ is indicated by the orientation of the turns with respect to the y -axis. If the center of the turn is pointing away from the positive y -direction then the sign on $\sigma_{skew,i}^2$ and $\Gamma_n^{(i)}$ is positive, if the center of the turn is pointing toward the positive y -direction then the sign on $\sigma_{skew,i}^2$ and $\Gamma_n^{(i)}$ is negative. In figure 3 the sign of $\sigma_{skew,i}^2$ and $\Gamma_n^{(i)}$ on the right turn is positive and the sign on the left turn is negative. The sign changes with each successive turn which indicates how the complementary turns can be used in a serpentine to mitigate against large variance development. The sign on $\sigma_{skew,i}^2$ and $\Gamma_n^{(i)}$ is always positive for a straight channel (after a turn) and a spiral. The spiral configuration does not allow for complementary turns and instead uses large turn radii to mitigate against large variance development. As the turn radius tends to large values, the turn can be well approximated as a straight channel as variance generation due to the race track effect becomes negligible.

Turns in microfluidic devices introduce variance into the concentration profile due to the non-uniform velocity across the width of the channel. This variance generation is quantified by

$$\sigma_{turn,j}^2 = \left(\frac{8\mu_m E_{app} w_c^3}{r_j D} \right)^2 \sum_{n=1,3,5,\dots}^{\infty} \frac{\Phi_n(t_j)}{(n\pi)^8} \quad (12)$$

where $\Phi_n(t_j) = -1 + e^{-(n\pi)^2 D t_j / w_c^2} + (n\pi)^2 D t_j / w_c^2$.

The term σ_{other}^2 in Eq. (9) refers to any other sources of variance not modeled by the convection-diffusion equation (8). For ELFSE DNA separations, drag tag polydispersity is a significant source of variance (Ren et al., 1999; Albrecht et al., 2011; Istivan, 2012). The drag tag polydispersity leads to variance generation as multiple DNA molecules of the same length migrate at different velocities while attached to drag tags of different sizes. Micelles drag tags are polydisperse but they are also dynamic aggregates of surfactant monomers. Over a sufficiently long time, each DNA molecule samples a range of different micelle sizes as the micelles continuously trades surfactant monomers and decompose and reconstruct over longer time scales (Rillaerts and Joos, 1982; Patist et al., 2002). This results in an effective micelle drag tag size distribution that is of low variance. The model for σ_{poly}^2 is derived using a propagation of error analysis

$$\sigma_{poly}^2 = \left(\frac{\partial x}{\partial \alpha} \right)^2 \sigma_{\alpha}^2 \quad (13)$$

The distance traveled by a DNA molecule after some time t is $x = \mu_m E_{app} t$ where μ_m is given by Eq. (3). Since micelles change their size dynamically, the observed variance σ_{α}^2 is the results of sampling N times from the

actual micelle size distribution, thus $\sigma_\alpha^2 = \sigma_{\text{micelle}}^2/N$. The sampling frequency, ν , is assumed constant thus $N = \nu t$. Furthermore, micelle polydispersity changes with size (Mukerjee, 1972). A model that captures this effect is derived assuming that relative standard deviation, $RSD = \sigma_{\text{micelle}}/\alpha$ is constant with respect to micelle size. The variance due to micelle drag tag polydispersity is

$$\sigma_{\text{poly}}^2 = B' \left(\frac{\alpha}{m + \alpha} \right)^2 \mu_m E_{\text{app}} L \quad (14)$$

where $B' = RSD^2/\nu$, μ_m is the electrophoretic mobility given by Eq. (3), E_{app} is the applied field strength, and L is the total length of the separation channel. All other sources of variance for micelle ELFSE in a microfluidic device that are not specified in Eq. (9) – (12) and Eq. (14) are neglected.

The run time for micelle ELFSE in a microfluidic device is set by the instant the longest DNA length of interest (the length of read) is resolved. At that instant, the entire microfluidic device is scanned by the snap-shot detection and every DNA length is detected. The minimum snap-shot run time can be found by solving the following non-convex optimization problem

$$\begin{aligned} \min_{\alpha, V_{\text{app}}, L_i, r_j} \quad & t_{\text{run}} = \frac{L}{\mu_0 E_{\text{app}}} \left(1 + \frac{\alpha}{m_{\text{LOR}}} \right) \\ \text{s.t.} \quad & \text{Eq. (2) – Eq. (6),} \\ & \text{Eq. (9) – Eq. (12), Eq. (14)} \\ & L = \sum_{i \in I} L_i \\ & 0 \leq \alpha \leq \alpha_{\text{max}} \\ & 0 \leq V_{\text{app}} \leq V_{\text{max}} \\ & g(L_i, r_j) \leq X_{\text{max}} \\ & h(r_j) \leq Y_{\text{max}} \\ & c(L_i, r_j) \leq 0 \end{aligned} \quad (15)$$

where M is the set of DNA lengths separated, m_{LOR} is the length of read, i.e. $m_{\text{LOR}} = \max\{M\}$. The constraints g , h , and c are geometric constraints that ensures that the microfluidic device fits the specified area and ensures that all the sections are contiguous, $g(L_i, r_j) = h(r_j) = 2r_j$, $\forall j \in J$ for a spiral or $g(L_i, r_i) = L_i + r_{i+1} + r_{i-1}$, $\forall i \in I$ and $h(r_j) = \sum_{j \in J} 2r_j$ for a serpentine, X_{max} and Y_{max} is the maximum length allowed for the horizontal and vertical side of the microfluidic device, respectively. A serpentine is assumed to have straight channels aligned in the horizontal direction. In addition, spirals have the constraint $c(L_i, r_j) = \delta r - (r_{j-1} - r_j)$, $\forall j \in J$, which prevents the turns from overlapping. For serpentes the constraint $c(L_i, r_j) = L_i - L_{i-1}$, $\forall i \in I$ guarantees connectivity between the turns and each straight channel. Because of the physical nature of this problem, the resolution constraint $R_m \leq 1.5$ is a monotonic function that decreases with decreasing m . This allows us to replace the constraint $R_m \leq 1.5$, $\forall m \in M$ with $R_{m_{\text{LOR}}} \leq 1.5$.

The parameters are specified to match DNA in a micelle solution, i.e. $\mu_0 = 2.7 \times 10^{-4}$ cm²/V-s, $D_1 = 3.6 \times 10^{-6}$ cm²/s, $\alpha_{\text{max}} = 502$ and $B' = 0.6$ msec (Istivan, 2012). The length of read m_{LOR} is chosen to be 425 bases which is common for DNA separations in forensic applications (Shi, 2006). The maximum dimensions of the device are set at $X_{\text{max}} = Y_{\text{max}} = 10$ cm. The minimum gap between turns

in a spiral δr is set at 0.1 cm, which allows for practical fabrication of the device (Culbertson et al., 2000). The maximum applied voltage is $V_{\text{max}} = 30$ kV.

For this work CONOPT v. 3.14V supplied in GAMS v. 23.6.2 was used to solve the NLP.

3. RESULTS AND DISCUSSION

In this section we show the results from solving NLP (15) for both spiral and serpentine configurations with a varying number of sections separating a length of read m_{LOR} of 425 bases. Figure 4 shows the optimal run time as the number of sections increases from 2 to 9. A section is defined as either a straight channel or a semi-circular turn. Serpentes alternate between straight channels and semi-circular turns while spirals use a series of semi-circular turns of decreasing radius. The NLP (15) is infeasible using only one section which implies that the separation is not possible within these design constraints. Under our set of

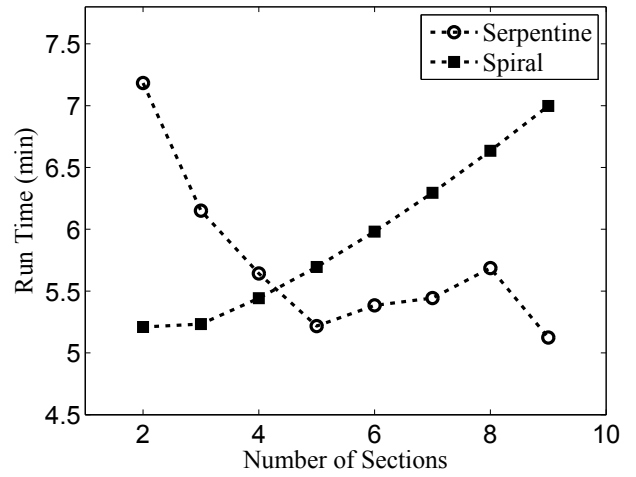


Fig. 4. Results from solving NLP (15) for spiral and serpentine configurations with a variable number of sections separating up to a length of read $m_{\text{LOR}} = 425$ bases. The minimum run time for the spiral is 5.2 minutes using two turn sections, while a serpentine requires 5.1 minutes using four turn sections and five straight sections. Both the serpentine and the spiral require at least two sections to produce feasible results.

design constraints, a serpentine using four turns and five straight sections is shown to be the minimum run time configuration for separating DNA using micelle ELFSE in a microfluidic device. The optimal serpentine configuration separates 425 bases of DNA in 5.1 minutes. In figure 4 we can see that the run time of a spiral increases as the number of turns increases. This is from requiring a full semi-circular turn with each additional turn section which have large radii to reduce turn variance. Turns of large radius better approximate straight channels and therefore reduce the variance introduced by the turn. The separation channel lengths for a varying number of turns for the spiral and serpentine configurations is shown in figure 5. A spiral is shown to have a longer optimal separation channel length than a serpentine. This result follows as spirals can use large turn radii to mitigate the effect of turn variance

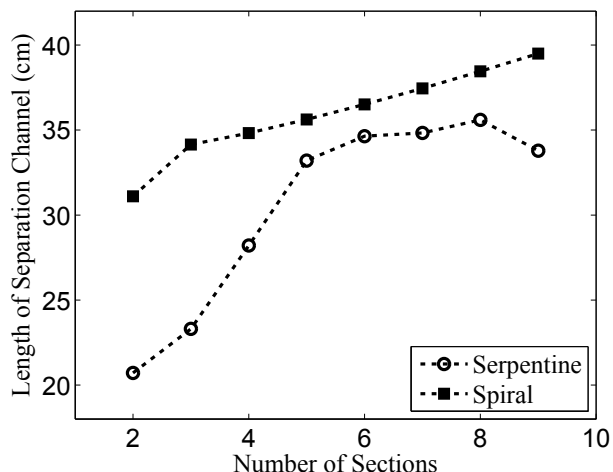


Fig. 5. Separation channel lengths. The separation channel length is sum of lengths of each section.

which leads to longer contour length. Serpentines are less efficient at fitting large radius turns into a small 10 cm × 10 cm area which results in less channel length available for the serpentine. Long channel lengths are generally desirable because they increase the spacing between DNA concentration bands. However they also lead to longer run times so the channels must be set sufficiently long to satisfy the resolution constraint $R_m \leq 1.5$ in the NLP (15) while maintaining the microfluidic device within the specified dimensions X_{max} and Y_{max} . The voltage as function

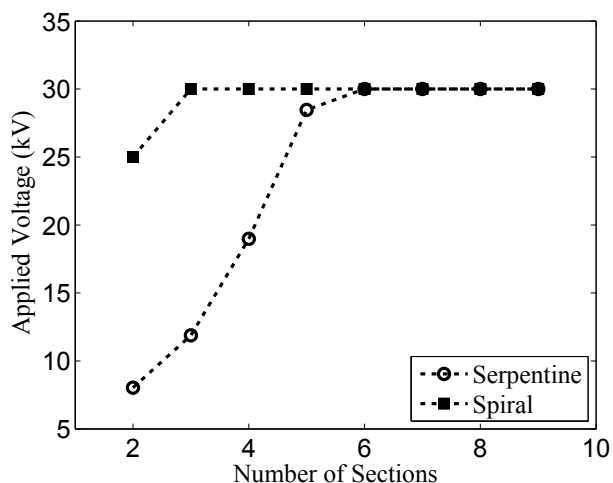


Fig. 6. Applied voltage in optimally designed spiral and serpentine configurations.

of the number of sections in the spiral and serpentine configurations is shown in figure 6. The design constraints were chosen so V_{max} is 30 kV. Figure 6 shows that this is an active constraint when a spiral has two or more turn sections or when a serpentine has six or more sections. The electric field results shown in figure 7 are proportional of the migration velocity of the DNA in the microfluidic device. Because the objective is to minimize run time, the optimal electric field must balance fast migration velocity against the resolution requirement.

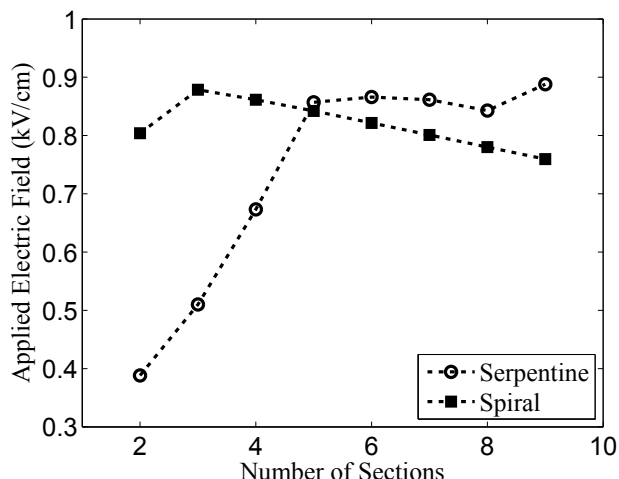


Fig. 7. Applied electric field strength in optimally designed spiral and serpentine configurations.

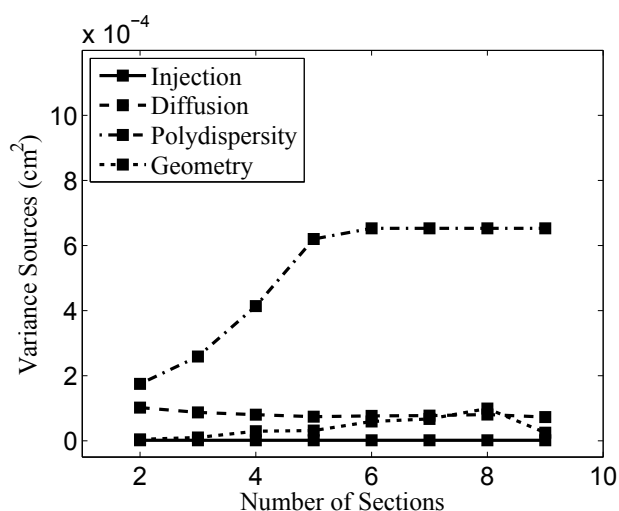


Fig. 8. Variance in optimally designed serpentine configuration.

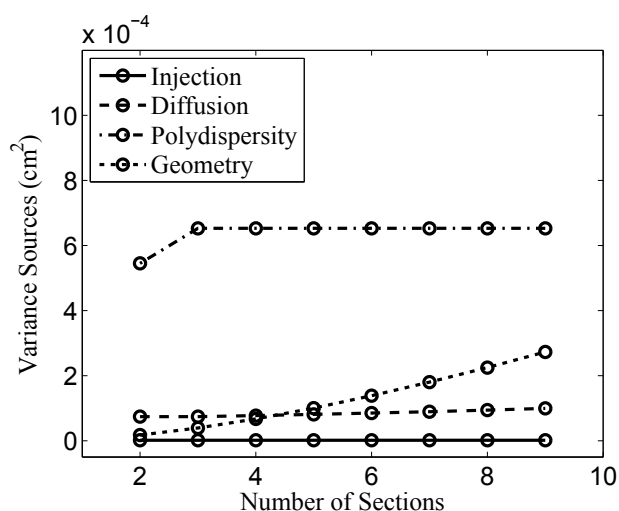


Fig. 9. Variance in optimally designed spiral configuration.

The optimal micelle size is 502 (α_{\max}) bases for every configuration in this work. Faster run times are, indeed, accessible with larger α_{\max} and lower micelle polydispersity B' which is currently an active area of research (Grosser et al., 2007; Savard et al., 2008; Istivan, 2012).

The variance sources for the serpentine and spiral configurations are shown in figure 8 and 9, respectively. Polydispersity is the most significant source of variance for both configurations.

4. CONCLUSIONS

In this paper we present a framework for determining the optimal configuration of a microfluidic device to separate DNA in minimum run time using the micelle end-labeled free solution electrophoresis technique. The non-linear programming problem is solved for a varying number of turn sections and straight sections to determine the optimal number of sections for both spiral and serpentine configurations. We found serpentine to be superior for separating DNA using micelle end-labeled free-solution electrophoresis. This work shows the utility of our framework for quickly differentiating between different DNA separation designs.

REFERENCES

- Albrecht, J.C., Kotani, A., Lin, J.S., Soper, S.A., and Barron, A.E. (2013). Simultaneous detection of 19 *K-ras* mutations by free-solution conjugate electrophoresis of ligase detection reaction products on glass microchips. *Electrophoresis*, 00, 1 – 8.
- Albrecht, J.C., Lin, J.S., and Barron, A.E. (2011). A 265-base DNA sequencing read by capillary electrophoresis with no separation matrix. *Analytical Chemistry*, 80, 509 – 515.
- Butler, J.M. (2001). *Forensic DNA Typing: Biology and Technology behind STR markers*. Academic Press, San Diego, CA, USA.
- Culbertson, C.T., Jacobson, S.C., and Ramsey, J.M. (1998). Dispersion sources for compact geometries on microchips. *Analytical Chemistry*, 70(18), 3781–3789.
- Culbertson, C.T., Jacobson, S.C., and Ramsey, J.M. (2000). Microchip devices for high-efficiency separations. *Analytical Chemistry*, 72(23), 5814–5819.
- Dorfman, K.D. (2010). DNA electrophoresis in microfabricated devices. *Reviews of Modern Physics*, 82, 2903 – 2947.
- Dorfman, K.D., King, S.B., Olson, D.W., Tree, J.D.P., and Tree, D.R. (2012). Beyond gel electrophoresis: Microfluidic separations, fluorescence, burst analysis, and DNA stretching. *Chemical Reviews*, doi: 10.1021.
- Griffiths, S.K. and Nilson, R.H. (2000). Band spreading in two-dimensional microchannel turns for electrokinetic species transport. *Analytical chemistry*, 72(21), 5473–5482.
- Grosser, S.T., Savard, J.M., and Schneider, J.W. (2007). Identification of PCR products using PNA amphiphiles in micellar electrokinetic chromatography. *Analytical Chemistry*, 79, 9513 – 9519.
- Istivan, S.B. (2012). *Gel-free Separations of DNA via Transient Attachment to Surfactant Micelles*. Ph.D. thesis, Carnegie Mellon University, Pittsburgh, PA 15213.
- Molho, J., Herr, A., Mosier, B., Santiago, J., Kenny, T., Brennen, R., Gordon, G., and Mohammadi, B. (2001). Optimization of turn geometries for microchip electrophoresis. *Analytical Chemistry*, 73(6), 1350–1360.
- Mukerjee, P. (1972). Size distribution of small and large micelles. multiple equilibrium analysis. *Journal of Physical Chemistry*, 76, 565 – 570.
- Patist, A., Kanicky, J.R., Shukla, P., and Shah, D.O. (2002). Importance of micellar kinetics in relation to technological processes. *Journal of Colloids and Interface Science*, 245, 1 – 15.
- Pfeiffer, A.J., Mukherjee, T., and Hauan, S. (2004). Design and optimization of compact microscale electrophoretic separation systems. *Industrial & Engineering Chemistry Research*, 43, 3539 – 3553.
- Ren, H., Karger, A., Oaks, F., Menchen, S., Slater, G., and Drouin, G. (1999). Separating DNA sequencing fragments without a sieving matrix. *Electrophoresis*, 20(12), 2501–2509.
- Rillaerts, E. and Joos, P.J. (1982). Rate of demicellization from the dynamic surface tensions of micellar solutions. *Journal of Physical Chemistry*, 86, 3471 – 3478.
- Sanger, F., Nicklen, S., and Coulson, A.R. (1977). DNA sequencing with chain-terminating inhibitors. *Proceedings of the National Academy of Sciences*, 74(12), 5463–5467.
- Savard, J.M., Grosser, S.T., and Schneider, J.W. (2008). Length-dependent DNA separations using multiple end-attached peptide nucleic acid amphiphiles in micellar electrokinetic chromatography. *Electrophoresis*, 29, 2779 – 2789.
- Shi, Y. (2006). DNA sequencing and multiplex STR analysis on plastic microfluidic devices. *Electrophoresis*, 27, 3703 – 3711.
- Viovy, J.L. (2000). Electrophoresis of DNA and other polyelectrolytes: Physical mechanisms. *Reviews of Modern Physics*, 72, 813–872.
- Wang, Y., Lin, Q., and Mukherjee, T. (2004). System-oriented dispersion models of general-shaped electrophoresis microchannels. *Lab on a Chip*, 4, 453 – 463.